

PDE-based Simulation of Thermal Distributions in Teeth by Conformal Parametrization

Martin Holzinger^{1*}, Pauline Steinkogler²

¹Institute of Analysis and Scientific Computing, TU Wien, Wiedner Hauptstraße 8-10, 1040 Vienna, Austria; *martin.holzinger@tuwien.ac.at

²BG XIII/1c, Fichtnergasse 15, 1130 Vienna, Austria; paulinsky.st@icloud.com

SNE 31(1), 2021, 1-8, DOI: 10.11128/sne.31.tn.10551
 Received: October 20, 2020; Revised: February 10, 2021;
 Accepted: February 20, 2021
 SNE - Simulation Notes Europe, ARGESIM Publisher Vienna,
 ISSN Print 2305-9974, Online 2306-0271, www.sne-journal.org

Abstract. With the conformal map from unit square to unit disk analytically known, in our last contribution we investigated ways to numerically map the disk to more general (but star-shaped) domains. Such point-mappings of the complex planes are now to be interpreted as transformations of co-ordinates, hence the domains are parametrized by the square. Using general, curvilinear co-ordinates one has to take the shape of the fundamental tensor and other related quantities into account. The also numerically known derivatives of the map act as metric quantities flowing in and correcting a pre-given PDE in Cartesian co-ordinates on such a domain. On the other hand, a formulation of physical laws in co-ordinate free manner gives an even smarter access to implement a simulation code of a given problem in *Mathematica*. In this article, we focus on a practical problem: let the domain be the cross-section of a tooth and the task be to find the temperature distribution on its boundary with respect to a heat source moving in the interior of the domain. This model can then be interpreted as a decision-finding issue to parameter identification when treating a tooth with a laser pulse. Considering the problem in three dimensions by using rotational symmetry will turn out to be essential with respect to the obtained results.

Introduction

The treatment of tooth root inflammations by root resection is (in the author's own experience) one of the less desirable aspects in the whole digestion process.

Moreover, success of this dolorous treatment can not be ensured and more commonly leads to extraction of the affected tooth after repeatedly abortive attempts.

To try to rescue a tooth from extraction anyhow, laser treatment can be applied as an alternative method.

The purpose of this alternative and widely painless endodontic laser treatment approach [1] is to annihilate malicious bacteria by means of thermal demolition with the obvious side condition that the *Parodontium* anchoring the tooth must not be damaged by temperatures too high. The area in question is sketched by the red line in Figure 1, labeled with *Cementum* there. For this undertaking, a laser source is moved along the root canal.

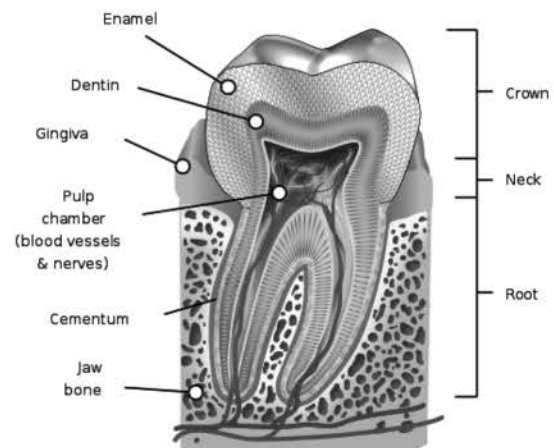


Figure 1: Schematic tooth cross-section (Source: Wikipedia).

With the gained knowledge of our previous articles (cf. [3] & [4]) we can set out to establish a simulation model on this issue. Hereto we adapt the developed heat equation simulation code on unit square (and unit disk) with the insights provided by the conformal map. While ba-

sically we are already ready-to-run, deducing a model in three spacial dimensions is most desirable. This extension has yet to be discussed as well as an apt implementation of the laser heat source. Moreover, let us focus on the temperature distribution on the boundary.

1 Calculating the Tooth Grid

In our previous contribution [4, p.90f], for three different pre-given domains we investigated how to numerically establish the function of boundary correspondence, $\varphi \mapsto \theta$, relating the angle φ circling around unit disk \mathfrak{E} to angle θ on domain \mathfrak{G} with given boundary \mathfrak{C} as a smooth, closed Jordan arc. Due to worst error behaviour we will focus on geometry *GEO3*, described by means of Hermite interpolation. This domain may be used to derive a tooth cross-section simulation grid.

1.1 Notation

Using Cartesian co-ordinates (ξ, η) on \mathfrak{G} , we assumed rotational symmetry with respect to η -axis. Introducing the complex ζ -plane, a point of \mathfrak{G} can be addressed via $\zeta = \xi + i\eta$ by means of its complex representation. Let then w denote the complex w -plane where \mathfrak{E} resides so its points are reached by the complex representation $w = u + iv$. Furthermore, in a third complex plane we represent the unit square \mathfrak{Q} in the z -plane, $z = x + iy$, where the computational grid is located (cf. [3, p.43]).

For the subsequent task to numerically construct the map $\overline{\mathfrak{Q}} \rightarrow \overline{\mathfrak{G}}$, the unit disk \mathfrak{E} will be interposed. Hence, let $w = h(z)$ be the elliptic function evolved in [3, p.47] acting as a closed-form conformal map $\mathfrak{Q} \rightarrow \mathfrak{E}$. We note that implementing and calculating h and its derivatives numerically with *Mathematica* is straight-forward.

Finally, with $\zeta = g(w)$ presented in [4, p.87] mapping the closures $\overline{\mathfrak{E}} \rightarrow \overline{\mathfrak{G}}$ we find the conformal map from square onto domain by composition of g and h , thus $f = g \circ h : \overline{\mathfrak{Q}} \rightarrow \overline{\mathfrak{G}}$ where $\zeta = f(z) = g(h(z))$.

It is well worth explicitly pointing out the chain rule for the case that $g(w) = w \cdot e^{P(w)}$ is established by means of a trigonometric polynomial (see again [4, p.87]),

$$P(w) = \frac{a_0}{2} + \sum (a_k - ib_k)w^k,$$

applying the first derivative then results in

$$f'(z) = \xi_x + i\eta_x = g'(w)h'(z) = h'(z)e^{P(w)}(wP'(w) + 1),$$

whereas for the second derivative we get

$$\begin{aligned} f''(z) &= \xi_{xx} + i\eta_{xx} = g''h'^2 + h''g' \\ &= e^P [h'' + P'(2h'^2 + wh'' + wh'^2P') + wh'^2P'']. \end{aligned}$$

Term by term differentiation of P is trivial for *Mathematica*, so is the numeric evaluation of f, f' and f'' .

1.2 Remarks on g and g'

Concerning trigonometric interpolation of $\ln \rho(\theta(\varphi))$ to get hold of the Fourier coefficients establishing the map g we noticed that series convergence degrades depending on the ε -condition as well as in case that slope discontinuities arise in the parametrization of \mathfrak{C} .

Of course, with *GEO3* we will not face any problems: smoothness of boundary is guaranteed by means of Hermite interpolation and the ε -condition has been investigated as well as convergence and error behaviour on $[0, 2\pi]$. But let us have a look at the non-trigonometric case in this section just for completeness.

For example, by considering the unit square itself as image domain \mathfrak{G} , in [4, p.89] we showed that high-precision $\theta(\varphi)$ can be achieved nonetheless by switching to more apt base functions than trigonometric ones.

Suppose therefore that $\theta(\varphi)$ is known to and implemented in *Mathematica* as well as $\rho(\theta)$ describing \mathfrak{C} is at hand. Then we distinguish four cases [5, p.56f] to snatch numeric values for g and g' :

Unit disk boundary point images:

$$g(e^{i\varphi}) = \rho(\theta(\varphi)) \cdot e^{i\theta(\varphi)}$$

Unit disk boundary point derivatives:

$$g'(e^{i\varphi}) = \theta'(\varphi) \cdot e^{i(\theta(\varphi)-\varphi)} \cdot [\rho(\theta(\varphi)) - i\rho'(\theta(\varphi))]$$

Unit disk interior point images:

$$g(w) = w \cdot \exp \left[\frac{1}{2\pi} \int_0^{2\pi} \ln \rho(\theta(\vartheta)) \frac{e^{i\vartheta} + w}{e^{i\vartheta} - w} d\vartheta \right]$$

Unit disk interior point derivatives:

$$g'(w) = \frac{g(w)}{w} + \frac{g(w)}{2\pi} \int_0^{2\pi} \frac{\ln \rho(\theta(\vartheta)) + i(\theta(\vartheta) - \vartheta)}{(e^{i\vartheta} - w)^2} e^{i\vartheta} d\vartheta.$$

$$g'(0) = \frac{1}{2i\pi} \oint_{\gamma} \frac{g(\zeta)}{\zeta(\zeta - 0)} d\zeta = \frac{1}{2\pi} \int_0^{2\pi} \frac{\rho(\theta(\vartheta))e^{i\theta(\vartheta)}}{e^{i\vartheta}} d\vartheta.$$

If necessary, formulae for higher-order derivatives can be developed likewise by regarding the generalized CAUCHY integral formula for derivatives [2, p.246, Theorem 4.7d] like we did for points in the interior of the unit disk to evaluate $g'(w)$. Finally note that the singularity arising in the origin, $g'(0)$, was removed by subsequent application of CAUCHY'S integral formula.

1.3 Grid Visualization

Setting up and saving the grids on unit square, disk and *GEO3* is done in complex arrays Z , W and $ZETA$:

```
For[i=1, i<=n, i++, For[j=1, j<=n, j++,
Z[[i, j]]=-1+(i-1) dx+I(-1+(j-1) dy);]];
X = Re[Z]; Y = Im[Z];
```

Real and imaginary parts of these arrays are also defined for the ease of data access. Whereas these objects are used in the simulation process (for example, Z can be fed directly in functions h and f and other arrays are defined to save the derivative values on the grid), the grids themselves are stored in separate structures:

```
Zgrid=Flatten[Table[
X[[i, j]], Y[[i, j]], i, 1, n, j, 1, n], 1];
```

With these definitions, `ListPlot` outputs can be generated in a convenient way. Figure 2 shows the result of such an output ($n = 101$). While Figure 3 has already been presented in [3, p.47], Figure 4 shows the image grid following from the conformal mapping f from square to *GEO3* with the unit disk interposed. Note in particular how the square corners are being mapped. Despite these present singularities no further impact on the simulation process can be expected.

In the visualization context, all of these mappings act as point transformations. In our subsequent examinations, f will alternatively be interpreted as a transformation of co-ordinates. With the metrics calculated in addition, we are ready to run a simulation model on the tooth cross-section parameterized by the unit square.

2 Setting up the Model

It is one of the major benefits of our approach in using conformal parametrization of a domain by means of the unit square that - as soon as the conformal map and its

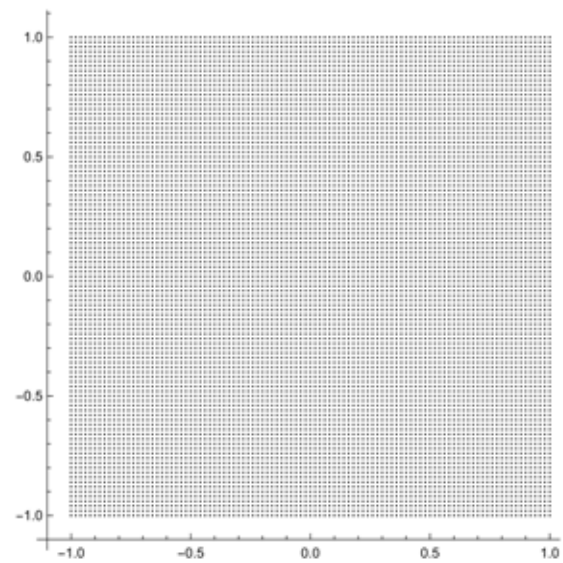


Figure 2: 101 × 101-point simulation grid in z -plane.

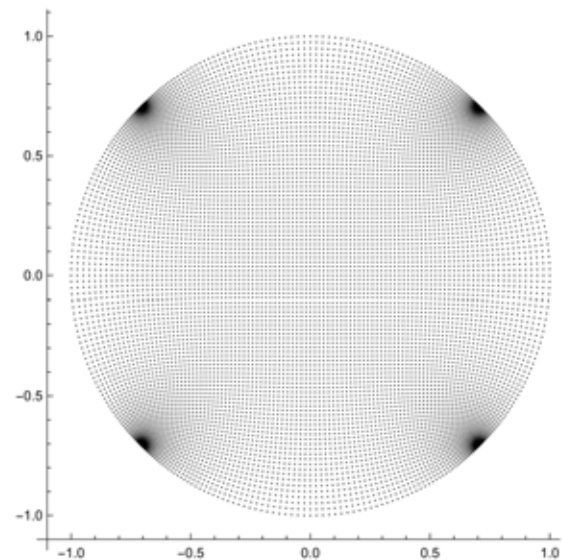


Figure 3: Result of the mapping $h: \overline{\mathcal{D}} \rightarrow \overline{\mathcal{E}}$ in w -plane.

derivatives are numerically determined and externally saved - an existing PDE-model can easily be ported to another domain of interest.

Basically, one starts with an investigation of the underlying PDE itself in co-ordinate free formulation. Regarding the fundamental tensor involved and knowing $g_{ij} = \delta_{ij}$ in Cartesian co-ordinates, the proper transformation laws have to be taken into account to determine its new shape as well as vector or tensor valued state variables must be transformed. Right here the conformal transformation f and its derivatives come into play.

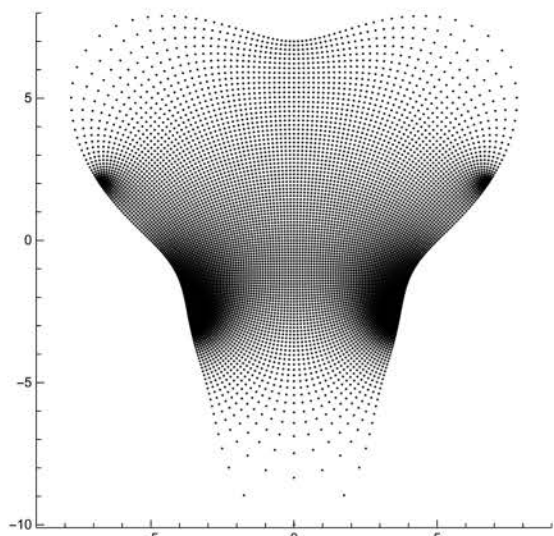


Figure 4: Result of the mapping $f = g \circ h : \bar{\Omega} \rightarrow \mathfrak{G}$ in ζ -plane.

2.1 3D considerations

Starting from what we have implemented so far considering the simulation models on square and disk, switching to our new f' paying tribute to domain *GEO3*, the heat equation on the tooth cross-section can be simulated and one might think that we are already done.

However, such an approach in two dimensions is worth to be critically impugned. In fact, dropping the third Cartesian co-ordinate, \mathfrak{z} , to work with a 2D model results in the assumption of a constant temperature profile in this direction. Thus, this proceeding will lead us to a 3D geometry similar to a rod with infinite length, having a cross-section \mathfrak{G} in each fixed point \mathfrak{z} .

This is definitely not in our intention and a comparison of mean temperature distributions will in fact reveal a 44% deviation with regard to the 3D model to be developed below. Let us therefore pack rotational symmetry by introducing cylindrical co-ordinates in our model to prevent dentists from having a formidable tooth braai.

Let thus be $\mathfrak{G}^* \subset \mathbb{R}^3$ a three-dimensional domain and $(\xi, \eta, \mathfrak{z})$ Cartesian co-ordinates with η denoting the axes of rotation. Let further be

$$f(x + iy) = \xi(x, y) + i\eta(x, y)$$

a conformal map such that for $\mathfrak{z} = 0$ the unit square in the (x, y) -plane is mapped to the cross-section $\mathfrak{G} \subset \mathfrak{G}^*$ located in the ζ -plane. Then the desired symmetry is incorporated by the co-ordinate transformation

$$\xi = \xi(x, y) \sin \varphi, \quad \eta = \eta(x, y), \quad \mathfrak{z} = \xi(x, y) \cos \varphi.$$

The new shape of the covariant metric tensor when switching from Cartesian to curvilinear co-ordinates, $(\xi, \eta, \mathfrak{z}) \rightarrow (x, y, \varphi)$, is determined by (cf. Figure 5)

$$\bar{g}_{ij} = \begin{pmatrix} \xi_x^2 + \eta_x^2 & 0 & 0 \\ 0 & \xi_x^2 + \eta_x^2 & 0 \\ 0 & 0 & \xi^2 \end{pmatrix}.$$

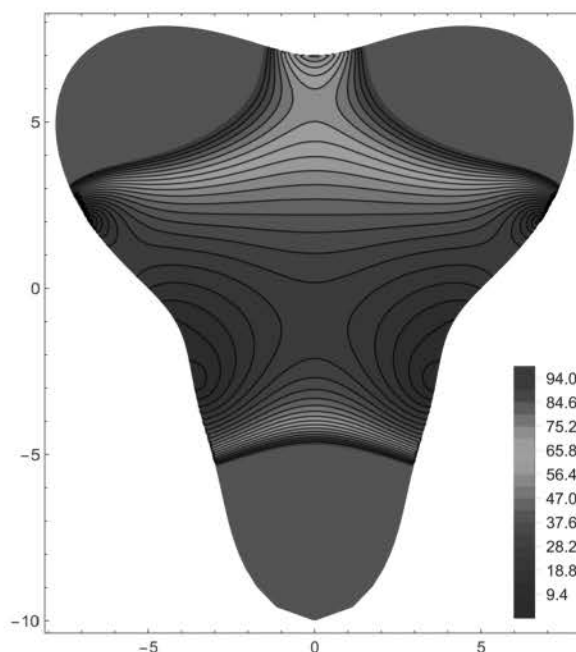


Figure 5: Fundamental tensor on \mathfrak{G} with $g_{11} = g_{22}$.

The transformation itself obviously has impacts on the expressions involved in differential operators, too. For example, examination of the LAPLACE operator given in [4, p.92] yields (let be $\chi = \xi_x^2 + \eta_x^2$)

$$\Delta u = \frac{1}{\chi} \left[\frac{\partial^2 u}{\partial x^2} + \frac{\partial^2 u}{\partial y^2} + \frac{1}{\xi} \left(\xi_x \frac{\partial u}{\partial x} - \eta_x \frac{\partial u}{\partial y} \right) \right] + \frac{1}{\xi^2} \frac{\partial^2 u}{\partial \varphi^2}.$$

The assumption of a rotational symmetric, angular constant temperature field now entitles us to drop the last summand in the expression above.

Comparing the remaining expression with the 2D simulation rod approach - the Laplacian is corrected by a factor $1/\chi$ in this case - we note that in addition, first derivatives of the temperature field $u(x, y, t)$ appear. Also, the sense of this expression on the axes of symmetry itself (singularity for $\xi = 0$) has to be questioned.

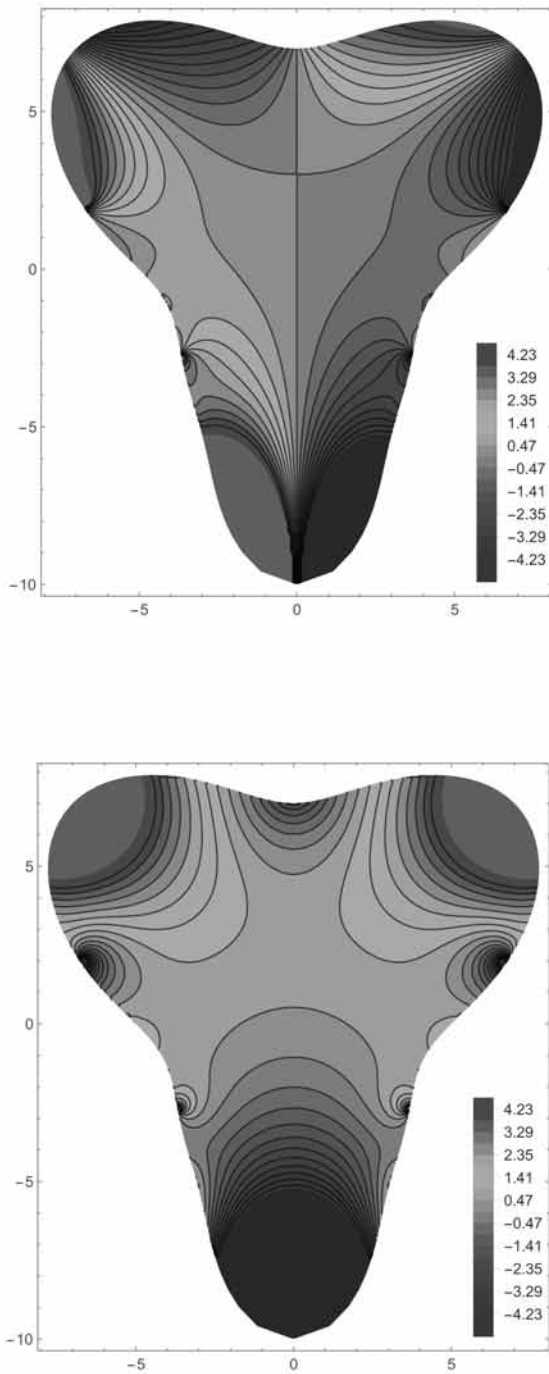


Figure 6: The two independent CHRISTOFFEL symbols Γ_{11}^1 (top) and Γ_{12}^1 (bottom) on tooth cross-section \mathfrak{G} can be derived by evaluating f' and f'' in each grid point.

In the course of setting up $f(z)$ by means of trigonometric interpolation, we also showed how to derive expressions for f' and f'' . With these functions implemented,

we are able to visualize the CHRISTOFFEL symbols shown in Figure 6. Although not needed for simulating the heat equation it is a good idea to calculate and externally save these numeric values for each grid point for the case that the base PDE has to be adapted.

2.2 Impacts on grid and model

As it can be expected that switching over to a 3D rotational geometry yields a far more realistic modeling approach, there are other good news concerning the grid size: the temperature field has to be η -symmetric per definition, meaning restricting the computational area to $[0,1] \times [-1,1]$ is sufficient. For an odd number n^2 of grid points on the unit square this results in a reduction to an effective number of $(n^2 + n)/2$ calculation points.

As an example, for the 101×101 -grid shown in Figure 2 instead of solving a system of 9.801 coupled ODEs we get along with 4.851 equations. This gain in simulation resources (primarily memory and CPU time) can be used for additional grid refinement if necessary.

These thoughts reflect the fact that the PDE itself only holds in the *interior* of the domain and one has to treat the boundary gridpoints in a different way. In this sense, the nature of reasonable boundary conditions in grid points $\zeta = i\eta, \eta \in [-1, 1]$ has yet to be clarified. Aside the axes of rotation we do not face any problems, DIRICHLET type conditions can be implemented as well as NEWTON/NEUMANN ones just like we previously did in our heat simulations on square and disk.

An heuristic approach to this boundary axes problem could claim smoothness of the temperature field when traversing the axes. This physically motivated demand would result in $\nabla_n u = 0 \forall \eta \in [-1, 1]$.

Finally, a mathematical approach can also legitimate prescription of the homogeneous NEUMANN boundary condition on the η -axes: with knowledge of the modified Laplacian holding in the interior, examination of

$$\lim_{\xi \rightarrow 0^+} (\xi_x u_x - \eta_x u_y) / \xi$$

reveals that zeroing the numerator is at least a necessary condition for the expression to make sense. Taking now into account that $\zeta = f(z)$ is η -symmetric, one first shows that the y -axes is mapped onto the η -axes. With $\xi(0,y) = 0, \xi_x(0,y) \neq 0$ and $\eta_x(0,y) = 0 \forall y$ comes $u_x = 0$ and we are done (details in [5, p.63, fn.6]).

2.3 Dental laser source

Introducing a heat source into our model to simulate the thermal treatment with a laser equipment inserted into the dental root canal with successive pulsing or movement can be done in different ways. With respect to rotational symmetry of our 3D model developed so far focusing on the η -axes (representing the canal) for the sake of not breaking up the symmetry seems reasonable.

One practicable approach could be altering the homogeneous NEUMANN boundary condition on the η -axes to $\nabla_{\mathbf{n}}u = \alpha(0, \eta, t)$. But aside the necessity of a correct parameter identification it is also to be expected that we are running into numerical problems with this modeling approach. Moreover, adjusting the depth of heat penetration would also be a desirable aspect but cannot be incorporated by this modeling procedure.

Seeming more flexible is the introduction of an additional source term into the heat equation itself which holds in the *interior* of the region. For this purpose, a Gaussian curve in two dimensions would be appropriate, that is we make use of

$$\sigma(\xi, \eta, t) = u_{amp} \cdot \exp \left[\frac{-\xi^2 - (\eta - \eta_0 - vt)^2}{s} \right]$$

as our heating source base signal function. Being dependent on both space and time variables this signal can then be further adjusted to the desired needs within a simulation run. For $t = 0$, the signal starts moving at point $(0, \eta_0)$ up- or downwards the axes of symmetry with velocity v (positive or negative).

Penetration depth is controlled by constant s . As for the amplitude u_{amp} , we leave the correct unit determination as well as considerations concerning plausible numeric values to the physicist. Having a look at the two-dimensional normal distribution can extend the signal to pay tribute to a certain direction (using correlation).

Furthermore we see that grid points on the η -axes will not be affected by this modeling approach, indeed the homogeneous NEUMANN boundary condition, $\nabla_{\mathbf{n}}u = 0$, has to hold during the whole simulation run. The peak u_{amp} of the Gaussian is calculated on the boundary by solving this condition *within simulation*.

Finally, caused by the fact that we are dealing with an invariant, adding the source term $\sigma(\xi, \eta, t)$ to the heat equation has no further impact concerning conformal transformation laws. Yet another advantage compared to heating via boundary condition where transformation of the normal vector has to be considered.

3 Parameters and Results

In [3, p.43] we assumed for κ , the coefficient of thermal diffusion being responsible for heat propagation, for sake of convenience $\kappa = 1$. This is by chance not too far from reality, in literature [7, Fig.5] one finds for dentine and enamel $\kappa \approx 2 - 5 \times 10^{-7} [m^2s^{-1}]$. Supposing $[mm]$ units like pointed out in the cross section figures thus entitles to define $\kappa = 0,3 [mm^2s^{-1}]$.

With $u_0 = 36^\circ C$ as prescribed initial temperature distribution the set of boundary conditions also has to be adapted to the level of this reference temperature u_0 ,

$$\nabla_{\mathbf{n}}u = \begin{cases} 0, & x = 0, y \in (-1, 1) \\ \alpha_r(u_0 - u), & x \in (0, 1), y = -1 \\ \alpha_r(u_0 - u), & x = 1, y \in (-1, 1) \\ \alpha_c(u_0 - u), & x \in (0, 1), y = 1. \end{cases}$$

Herein, for convenience the junction point from root to crown was determined to be – in computational coordinates (x, y) – at point $(1, 1)$. With α_c and α_r being positive heat is being dissipated to the exterior. For the heat transition coefficients (α_c : enamel→air and root α_r : cementum→bone) one finds in literature [6, p.1640] $\alpha_r = 10^{-4} [Wmm^{-2}K^{-1}]$ and $\alpha_c = 10^{-5} [Wmm^{-2}K^{-1}]$.

Using a canonical model first, impact of the different geometries on the results and rate of convergence can be studied. Mean temperatures and temperatures at $\zeta = 0$ for different grid spacing are presented in Table 1.

Finally, for the results shown in Figure 7, a constantly emitting heating source with $u_{amp} = 400$ and $s = 2/10$ was placed at $t = 0$ in point $\zeta = 5i$. Moving down the axes of symmetry with velocity $v = -1/5$, the point $\zeta = -7i$ is reached within $t = 60s$.

Geo	Grid	$u(0)$	$\Delta\%$	$u\emptyset$	$\Delta\%$
1	26×51	0.5076	—	0.4637	—
	51×101	0.5079	0.05	0.4649	0.25
	101×201	0.5079	0.005	0.4654	0.1
2	1.326	0.298	—	0.2745	—
	5.151	0.2988	0.285	0.2761	0.59
	20.301	0.299	0.047	0.2765	0.16
3	1.326	0.1975	—	0.1875	—
	5.151	0.1998	1.17	0.1905	1.6
	20.301	0.2004	0.283	0.1913	0.42

Table 1: Investigating convergence ($t = 50$) on the three different cross-sections presented in [4, p.91].

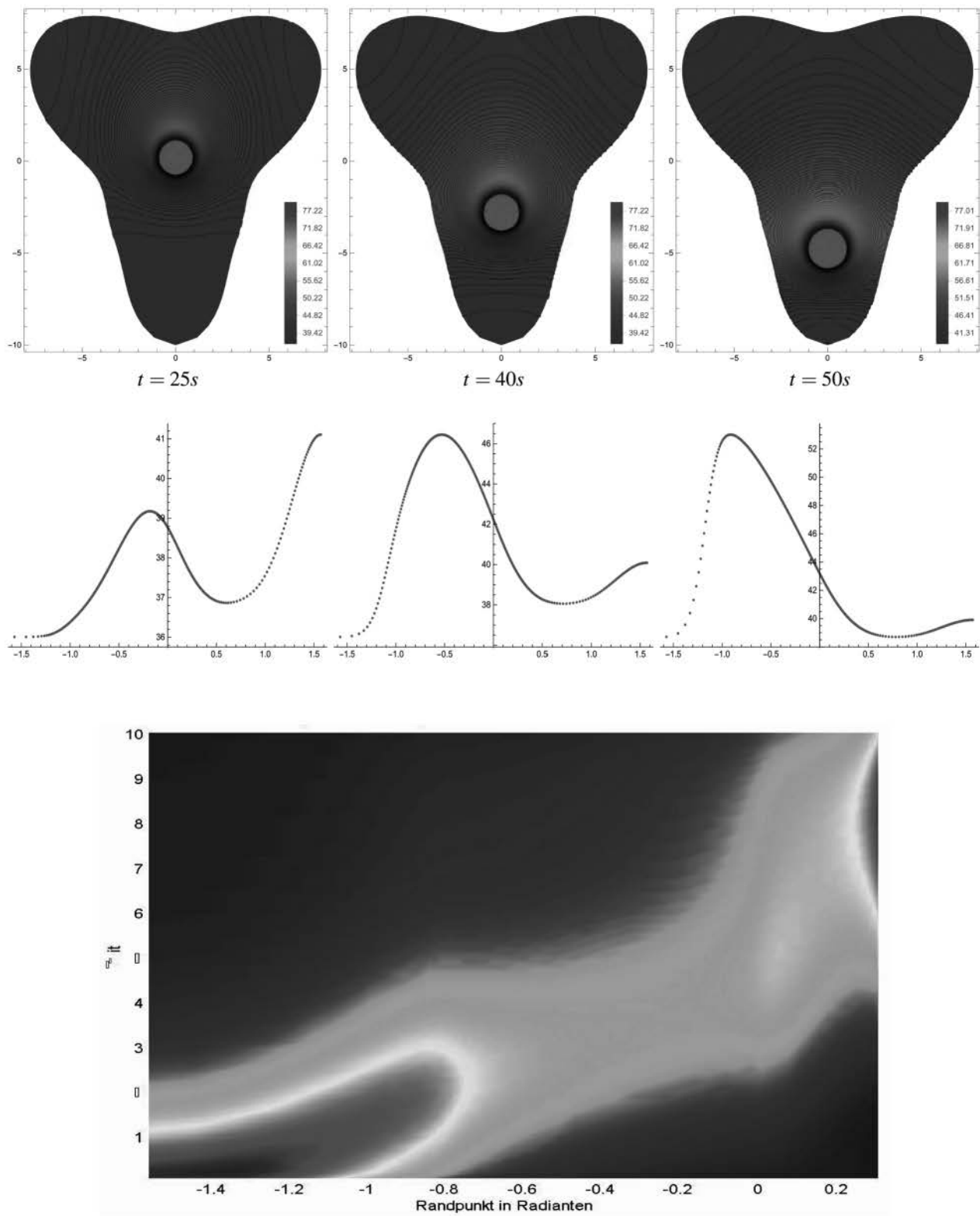


Figure 7: Simulation results: Isothermal lines for a heat source moving down from $\eta = 5$ to $\eta = -7$ (t) and associated temperature distributions on the boundary (c). Visualization on the boundary with time proceeding (b).

Summary

The present *SNE* article completes our conformal transformation simulation trilogy where it was our intention to point out an alternative approach to the classical method of Finite Elements by using Finite Differences on particular curvilinear grids to produce a system of coupled ordinary differential equations.

Hence, we demonstrated how conformal mappings are utilized to simulate two-dimensional or symmetric three-dimensional Initial Boundary Value Problems. Parametrization of a 2D-region by means of the unit square is achieved when combining the analytically given map from square to unit disk with numerically constructed conformal transformations. The introduction of such special co-ordinates thus makes the usage of rectangular structured computational grids possible.

The method of lines (we also focused on deriving generalized expressions for the sake of extensible approximation quality) can then be used to transform a given system of PDEs to a system of ODEs. The latter can be treated by standard methods available for systems with lumped parameters. All computations were carried out by using the program *Mathematica 11.3*.

Starting with Cartesian co-ordinates, linking up the derivatives of the map with the fundamental tensor is all to be done to get access to the metrics of the transformation. This approach proves to be highly flexible concerning an application to a wide range of PDEs.

In contrary, as theory of conformal mapping is bound to complex analysis, the field of application *a priori* is limited to two-dimensional domains which can be considered as a serious restriction. Knowing the special shape of the metric tensor in the conformal case, an attempt to construct an analogon in three dimensions would be an interesting topic for future research indeed.

Focusing on a thermal heat conduction problem for tooth laser treatment at last, the calculated temperature distribution on the boundary can be used to adjust source intensity for the sake of avoiding injuries. Possible further model extensions are discussed in [5, p.67ff].

References

- [1] Douschan, P. *Benefit der Anwendung des Diodenlasers in der Endodontie*. Med. Univ. Graz, diploma thesis (in German), 2014.
- [2] Henrici, P. *Applied and Computational Complex Analysis, Volume I*. John Wiley & Sons, New York-London-Sydney-Toronto 1974, ISBN 0-471-37244-7.
- [3] Holzinger, M. *CTDS – Mauling Heat Equation on Unit Disk by Conformal Parametrization*. *Simulation Notes Europe* 2020; 30(2): 43-50. DOI: 10.11128/sne.30.tn.10511.
- [4] Holzinger, M. *CTDS – High Precision Conformal Map of the Unit Disk to Star-Shaped Domains*. *Simulation Notes Europe* 2020; SNE 30(3): 85-94. DOI: 10.11128/sne.30.tn.10521.
- [5] Holzinger, M. *Konforme Abbildungen zur Simulation von Modellen mit verteilten Parametern*. Dissertation/PhD (in German), Wien, 2020. <http://katalog.ub.tuwien.ac.at/AC15652638>
- [6] Martins, M.A., Oliveira, L.S., Valle R.M. *Adaptivity for finite volume on unstructured triangular meshes: a study on thermal injury in teeth*. *International Journal for Numerical Methods in Engineering*, 2004; 61(10): 1625-1643.
- [7] Panas, A.J., Żmuda, S., Terpiłowski, J., Preiskorn, M. *Investigation of the Thermal Diffusivity of Human Tooth Hard Tissue*. *Intl. Journal of Thermophysics*, Vol. 24, Number 3, pp. 837-848, 2003. Online ISSN 1572-9567.